

SliceNStitch: Continuous CP Decomposition of Sparse Tensor Streams

Taehyung Kwon^{*†}, Inkyu Park^{*†}, Dongjin Lee[§], and Kijung Shin^{†§}

[†]Graduate School of AI and [§]School of Electrical Engineering, KAIST, Daejeon, South Korea
 {taehyung.kwon, inkyupark, dongjin.lee, kijungs}@kaist.ac.kr

Abstract—Consider traffic data (i.e., triplets in the form of source-destination-timestamp) that grow over time. Tensors (i.e., multi-dimensional arrays) with a time mode are widely used for modeling and analyzing such multi-aspect data streams. In such tensors, however, new entries are added only once per period, which is often an hour, a day, or even a year. This discreteness of tensors has limited their usage for real-time applications, where new data should be analyzed instantly as it arrives.

How can we analyze time-evolving multi-aspect sparse data ‘continuously’ using tensors where time is ‘discrete’? We propose SLICENSTITCH for continuous CANDECOMP/PARAFAC (CP) decomposition, which has numerous time-critical applications, including anomaly detection, recommender systems, and stock market prediction. SLICENSTITCH changes the starting point of each period adaptively, based on the current time, and updates factor matrices (i.e., outputs of CP decomposition) instantly as new data arrives. We show, theoretically and experimentally, that SLICENSTITCH is (1) *‘Any time’*: updating factor matrices immediately without having to wait until the current time period ends, (2) *Fast*: with constant-time updates up to 464× faster than online methods, and (3) *Accurate*: with fitness comparable (specifically, 72 – 100%) to offline methods.

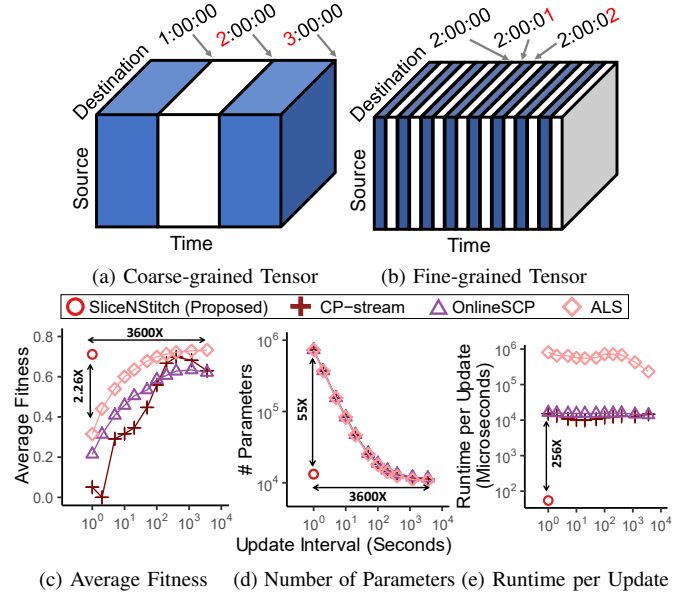
I. INTRODUCTION

Tensors (i.e., multidimensional arrays) are simple but powerful tools widely used for representing time-evolving multi-aspect data from various fields, including bioinformatics [1], data mining [2], [3], text mining [4], and cybersecurity [5], [6]. For example, consider a traffic dataset given as triplets in the form of (source, destination, timestamp). The dataset is naturally represented as a 3-mode tensor whose three modes correspond to sources, destinations, and time ranges, respectively (see Fig. 1a and 1b). Each (i, j, k) -th entry of the tensor represents the amount of traffic from the i -th source to the j -th destination during the k -th time range.

Once we represent data as a tensor, many tools [7]–[10] are available for tensor analysis, and CANDECOMP/PARAFAC decomposition (CPD) [7] is one of the most widely used tools. Given an M -mode tensor, CPD gives a low-rank approximation, specifically a sum of few outer products of M vectors, which form M factor matrices. CPD has been used for various applications, and many of them, including anomaly detection [2], recommendation [11], [12], stock market prediction [13], and weather forecast [14], are time-critical.

While tensors and CPD are powerful tools, they are not suitable for real-time applications since time in them advances in a discrete manner, specifically once per period. For example,

^{*}Equal Contribution



(f) Summary: SLICENSTITCH is fast, space-efficient, and accurate.

Fig. 1. Advantages of SLICENSTITCH. (a) (b) Coarse-grained and fine-grained tensors where update intervals are 1 hour and 1 second, respectively. (c) (d) Given a tensor stream (see Section VI-B for detailed experimental settings), SLICENSTITCH updates factor matrices (i.e., outputs of CPD) instantly (i.e., with a short update interval) while achieving high fitness with a small number of parameters. (e) Even runtime per update is shorter in SLICENSTITCH than in the three considered methods based on conventional CPD. (f) A summary of the comparisons in (c) and (d).

in the tensor in Fig. 1a, each slice represents the amounts of traffic for one hour, and thus the tensor grows with a new slice only once per hour. That is, it may take one hour for new traffic to be applied to the tensor. For instance, traffic occurring at 2:00:01 is applied to the tensor at 3:00:00. Due to this discreteness, the outputs of CPD (i.e., factor matrices) are updated also only once per period even if incremental algorithms [15]–[17] are used.

How can we perform CPD ‘continuously’ for real-time applications? A potential solution is to make the granularity of the time mode extremely fine. According to our preliminary studies, however, it causes the following problems:

- **Degradation of Fitness (Fig. 1c)** An extremely fine-grained

time mode results in an extremely sparse tensor, which is known to be of high rank [18], and thus it degrades the fitness of the low-rank approximation, such as conventional CPD. As shown in Fig. 1c, the finer the time mode is, the lower the fitness of CPD is.

- **Increase in the Number of Parameters (Fig. 1d):** The parameters of CPD are the entries of factor matrices, as explained in Section II, and the size of each factor matrix is proportional to the length of the corresponding mode of the input tensor. An extremely fine-grained time mode leads to an extremely long time mode and thus extremely many parameters, which require huge computational and storage resources. As shown in Fig. 1d, the finer the time mode is, the more parameters CPD requires.

In this work, we propose SLICENSTITCH for continuous CPD without increasing the number of parameters. It consists of a data model and online algorithms for CPD. From the **data model aspect**, we propose the continuous tensor model for time-evolving tensors. In the model, the starting point of each period changes adaptively, based on the current time, so that newly arrived data are applied to the input tensor instantly. From the **algorithmic aspect**, we propose a family of online algorithms for CPD of sparse tensors in the continuous tensor model. They update factor matrices instantly in response to each change in an entry of the input tensor. To the best of our knowledge, they are the first algorithms for this purpose, and existing online CPD algorithms [15]–[17] update factor matrices only once per period. We summarize our contributions as follows:

- **New data model:** We propose the continuous tensor model, which allows for processing time-evolving tensors continuously in real-time for time-critical applications.
- **Fast online algorithms:** We propose the first online algorithms that update outputs of CPD instantly in response to changes in an entry. Their fitness is comparable (specifically, 72 – 100%) even to offline competitors, and an update by them is up to 464× faster than that of online competitors.
- **Extensive experiments:** We extensively evaluate our algorithms on 4 real-world sparse tensors, and based on the results, we provide practitioner’s guides to algorithm selection and hyperparameter tuning.

Reproducibility: The code and datasets used in the paper are available at <https://github.com/DMLab-Tensor/SliceNStitch>.

Remarks: CPD may not be the best decomposition model for tensors with time modes, and there exist a number of alternatives, such as Tucker, INDSCAL, and DEDICOM (see [19]). Nevertheless, as a first step, we focus on making CPD ‘continuous’ due to its prevalence and simplicity. We leave extending our approach to more models as future work.

In Section II, we introduce some notations and preliminaries. In Section III, we provide a formal problem definition. In Sections IV and V, we present the model and optimization algorithms of SLICENSTITCH, respectively. In Section VI, we review our experiments. After discussing some related works in Section VII, we conclude in Section VIII.

TABLE I
TABLE OF FREQUENTLY-USED SYMBOLS

Symbol	Definition
\mathbf{A}	a matrix
$\mathbf{A}(i, :), \mathbf{A}(:, i)$	i -th row of \mathbf{A} , i -th column of \mathbf{A}
$\mathbf{A}', \mathbf{A}^\dagger$	transpose of \mathbf{A} , pseudoinverse of \mathbf{A}
$\odot, *$	Khatri-Rao product, Hadamard product
\mathcal{X}	a tensor
M	order of \mathcal{X}
N_m	number of indices in the m -th mode of \mathcal{X}
x_{i_1, i_2, \dots, i_M}	(i_1, i_2, \dots, i_M) -th entry of \mathcal{X}
$ \mathcal{X} $	number of non-zeros of \mathcal{X}
$\ \mathcal{X}\ _F$	Frobenius norm of \mathcal{X}
$\mathbf{X}_{(m)}$	mode- m matricization of \mathcal{X}
R	rank of CPD
$\mathbf{A}^{(m)}$	factor matrix of the m -th mode
$\tilde{\mathcal{X}}$	an approximation of \mathcal{X} by CPD
$\mathcal{D}(t, W)$	tensor window at time t
$\Delta\mathcal{X}$	a change in \mathcal{X}
W	number of indices in the time mode
$\text{deg}(m, i_m)$	number of non-zeros with m -th mode index i_m
$a_{ij}^{(m)}$	(i, j) -th entry of $\mathbf{A}^{(m)}$

II. PRELIMINARIES

In this section, we introduce some notations and preliminaries. Some frequently-used symbols are listed in Table I.

Basic Notations: Consider a matrix \mathbf{A} . We denote its i -th row by $\mathbf{A}(i, :)$ and its i -th column by $\mathbf{A}(:, i)$. We denote the transpose of \mathbf{A} by \mathbf{A}' and the Moore-Penrose pseudoinverse of \mathbf{A} by \mathbf{A}^\dagger . We denote the Khatri-Rao and Hadamard products by \odot and $*$, respectively. See Section I of [20] for the definitions of the Moore-Penrose pseudoinverse and both products.

Consider an M -mode sparse tensor $\mathcal{X} \in \mathbb{R}^{N_1 \times N_2 \times \dots \times N_M}$, where N_m denotes the length of the m -th mode. We denote each (i_1, i_2, \dots, i_M) -th entry of \mathcal{X} by x_{i_1, i_2, \dots, i_M} . We let $|\mathcal{X}|$ be the number of non-zero entries in \mathcal{X} , and we let $\|\mathcal{X}\|_2$ be the Frobenius norm of \mathcal{X} . We let $\mathbf{X}_{(m)}$ be the matrix obtained by matricizing \mathcal{X} along the m -th mode. See Section I of [20] for the definitions of the Frobenius norm and matricization.

CANDECOMP/PARAFAC Decomposition (CPD): Given an M -mode tensor $\mathcal{X} \in \mathbb{R}^{N_1 \times N_2 \times \dots \times N_M}$ and rank $R \in \mathbb{N}$, CANDECOMP/PARAFAC Decomposition (CPD) [7] gives a rank- R approximation of \mathcal{X} , expressed as the sum of R rank-1 tensors (i.e., outer products of vectors) as follows:

$$\begin{aligned} \mathcal{X} &\approx \sum_{r=1}^R \mathbf{a}_r^{(1)} \circ \mathbf{a}_r^{(2)} \circ \dots \circ \mathbf{a}_r^{(M)}, \\ &\equiv \sum_{r=1}^R \mathbf{A}^{(1)}(:, r) \circ \mathbf{A}^{(2)}(:, r) \circ \dots \circ \mathbf{A}^{(M)}(:, r), \\ &\equiv \llbracket \mathbf{A}^{(1)}, \mathbf{A}^{(2)}, \dots, \mathbf{A}^{(M)} \rrbracket \equiv \tilde{\mathcal{X}}, \end{aligned} \quad (1)$$

where $\mathbf{a}_r^{(m)} \in \mathbb{R}^{N_m}$ for all $r \in \{1, 2, \dots, R\}$, and \circ denotes the outer product (see Section I of [20] for the definition). Each $\mathbf{A}^{(m)} \equiv [\mathbf{a}_1^{(m)} \ \mathbf{a}_2^{(m)} \ \dots \ \mathbf{a}_R^{(m)}] \in \mathbb{R}^{N_m \times R}$ is called the *factor matrix* of the m -th mode.

CP decomposition aims to find factor matrices that minimize the difference between the input tensor \mathcal{X} and its approximation

$\tilde{\mathcal{X}}$. That is, it aims to solve Eq. (2).

$$\min_{\mathbf{A}^{(1)}, \dots, \mathbf{A}^{(M)}} \left\| \mathcal{X} - \llbracket \mathbf{A}^{(1)}, \mathbf{A}^{(2)}, \dots, \mathbf{A}^{(M)} \rrbracket \right\|_F, \quad (2)$$

where $\|\cdot\|_F$ is the Frobenius norm (see Section I of [20] for the definition).

Alternating Least Squares (ALS): Alternating least squares (ALS) [8], [21] is a standard algorithm for computing CPD of a static tensor. For each n -th mode, $\llbracket \mathbf{A}^{(1)}, \mathbf{A}^{(2)}, \dots, \mathbf{A}^{(M)} \rrbracket_{(n)} = \mathbf{A}^{(n)} (\odot_{m \neq n}^M \mathbf{A}^{(m)})'$, and thus the mode- n matricization of Eq. (2) becomes

$$\min_{\mathbf{A}^{(1)}, \dots, \mathbf{A}^{(M)}} \left\| \mathbf{X}_{(n)} - \mathbf{A}^{(n)} (\odot_{m \neq n}^M \mathbf{A}^{(m)})' \right\|_F. \quad (3)$$

While the objective function in Eq. (3) is non-convex, solving Eq. (3) only for $\mathbf{A}^{(n)}$ while fixing all other factor matrices is a least-square problem. Finding $\mathbf{A}^{(n)}$ that makes the derivative of the objective function in Eq. (3) with respect to $\mathbf{A}^{(n)}$ zero leads to the following update rule for $\mathbf{A}^{(n)}$:

$$\mathbf{A}^{(n)} \leftarrow \mathbf{X}_{(n)} (\odot_{m \neq n}^M \mathbf{A}^{(m)}) \{ *_{m \neq n}^M \mathbf{A}^{(m)'} \mathbf{A}^{(m)} \}^\dagger. \quad (4)$$

ALS performs CPD by alternatively updating each factor matrix $\mathbf{A}^{(n)}$ using Eq. (4) until convergence.

III. PROBLEM DEFINITION

In this section, we first define multi-aspect data streams. Then, we describe how it is typically modeled as a tensor and discuss the limitation of the common tensor modeling method. Lastly, we introduce the problem considered in this work.

Multi-aspect Data Stream and Examples: We define a multi-aspect data stream, which we aim to analyze, as follows:

Definition 1 (Multi-aspect Data Stream). A *multi-aspect data stream* is defined as a sequence of timestamped M -tuples $\{(e_n = (i_1, \dots, i_{M-1}, v_n), t_n)\}_{n \in \mathbb{N}}$, where i_1, \dots, i_{M-1} are categorical variables, $v_n \in \mathbb{R}$ is a numerical variable, and $t_n \in \mathbb{N}$ is the time (e.g., Unix timestamp) when the n -th tuple e_n occurs. We assume that the sequence is chronological, i.e.,

$$t_n \leq t_m \text{ if } n < m.$$

For simplicity, we also assume that the categorical variables are also (assigned to) integers, i.e.,

$$i_m \in \{1, \dots, N_m\}, \quad \forall m \in \{1, \dots, M-1\}.$$

Time-evolving data from various domains are naturally represented as a multi-aspect data stream as follows:

- **Traffic History:** Each 3-tuple $e_n = (\text{source}, \text{destination}, 1)$ indicates a trip that started at time t_n .
- **Crime History:** Each 3-tuple $e_n = (\text{location}, \text{type}, 1)$ indicates an incidence of crime at time t_n .
- **Purchase History:** Each 4-tuple $e_n = (\text{user}, \text{product}, \text{color}, \text{quantity})$ indicates a purchase at time t_n .

Common Tensor Modeling Method and its Limitations:

Multi-aspect data streams are commonly modeled as tensors to benefit from powerful tensor analysis tools (e.g., CP decomposition) [16], [17], [22]–[27]. Specifically,

a multi-aspect data stream is modeled as an M -mode tensor $\mathcal{X} \in \mathbb{R}^{N_1 \times \dots \times N_{M-1} \times W}$, where W is the number of indices in the time mode (i.e., the M -th mode). For each $w \in \{1, \dots, W\}$, let $\mathcal{G}_w \in \mathbb{R}^{N_1 \times N_2 \times \dots \times N_{M-1}}$ be the $(M-1)$ -mode tensor obtained from \mathcal{X} by fixing the M -th mode index to w . That is, $\mathcal{X} \equiv \mathcal{G}_1 \parallel \dots \parallel \mathcal{G}_{W-1} \parallel \mathcal{G}_W$, where \parallel denotes concatenation. Each tensor \mathcal{G}_w is the sum over T time units (i.e., T is the period) ending at wT . That is, each (j_1, \dots, j_M) -th entry of \mathcal{G}_w is the sum of v_n over all M -tuples e_n where $i_m = j_m$ for all $m \in \{1, \dots, M-1\}$ and $t_n \in (wT - T, wT]$. See Figs. 1a and 1b for examples where T is an hour and a second, respectively. As new tuples in the multi-aspect data stream arrive, a new $(M-1)$ -mode tensor is added to \mathcal{X} once per period T .

Additionally, in many previous studies on window-based tensor analysis [22]–[24], [26], the oldest $(M-1)$ -mode tensor is removed from \mathcal{X} once per period T to fix the number of indices in the time mode to W . That is, at time $t = W'T$ where $W' \in \{W+1, W+2, \dots\}$, $\mathcal{X} \equiv \mathcal{G}_{W'-W+1} \parallel \dots \parallel \mathcal{G}_{W'-1} \parallel \mathcal{G}_{W'}$.

A serious limitation of this widely-used tensor model is that the tensor \mathcal{X} changes only once per period T while the input multi-aspect data stream grows continuously. Thus, it is impossible to analyze multi-aspect data streams continuously in real time in response to the arrival of each new tuple.

Problem Definition: How can we continuously analyze multi-aspect data streams using tensor-analysis tools, specifically, CPD? We aim to answer this question, as stated in Problem 1.

Problem 1 (Continuous CP Decomposition). **(1) Given:** a multi-aspect data stream, **(2) to update:** its CP decomposition instantly in response to each new tuple in the stream, **(3) without having to wait** for the current period to end.

Note that, as discussed in Section I and shown in Fig. 1, an extremely short period T cannot be a proper solution since it extremely decreases the fitness of CPD and at the same time increases the number of parameters.

IV. PROPOSED DATA MODEL AND IMPLEMENTATION

In this section, we propose the continuous tensor model and its efficient implementation. This data model is one component of SLICENSTITCH. See Section V for the other component.

A. Proposed Data Model: Continuous Tensor Model

We first define several terms which our model is based on.

Definition 2 (Tensor Slice). Given a multi-aspect data stream (Definition 1), for each timestamped M -tuple $(e_n = (i_1, \dots, i_{M-1}, v_n), t_n)$, we define the *tensor slice* $\mathcal{Z}_n \in \mathbb{R}^{N_1 \times \dots \times N_{M-1}}$ as an $(M-1)$ -mode tensor where the (i_1, \dots, i_{M-1}) -th entry is v_n and the other entries are zero.

Definition 3 (Tensor Unit). Given a multi-aspect data stream, a time t , and the period T , we define the *tensor unit* \mathcal{Y}_t as

$$\mathcal{Y}_t \equiv \sum_{t_n \in (t-T, t]} \mathcal{Z}_n.$$

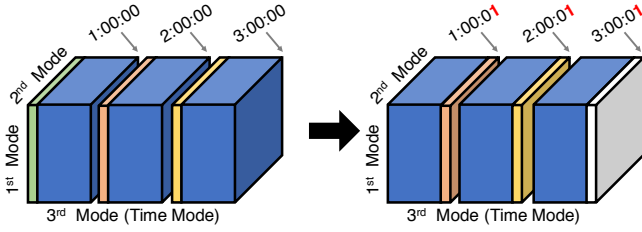


Fig. 2. **Example of the continuous tensor model.** The starting points of tensor units (whose length is an hour) change adaptively based on the current time (which is 3:00:01).

That is, $\mathcal{Y}_t \in \mathbb{R}^{N_1 \times \dots \times N_{M-1}}$ is an aggregation of the tuples occurred within the half-open interval $(t - T, t]$.

Definition 4 (Tensor Window). Given a multi-aspect data stream, a time t , the period T , and the number of time-mode indices W , we define the *tensor window* $\mathcal{D}(t, W)$ as

$$\mathcal{D}(t, W) \equiv \mathcal{Y}_{t-(W-1)T} \parallel \dots \parallel \mathcal{Y}_{t-T} \parallel \mathcal{Y}_t,$$

where \parallel denotes concatenation.

That is, $\mathcal{D}(t, W) \in \mathbb{R}^{N_1 \times \dots \times N_{M-1} \times W}$ concatenates the W latest tensor units.

The main idea of the continuous tensor model is to adaptively adjust the starting point (or equally the end point) of each tensor unit based on the current time, as described in Definition 5 and Fig. 2.

Definition 5 (Continuous Tensor Model). In the *continuous tensor model*, given a multi-aspect data stream, the period T , and the number of time-mode indices W , the modeled tensor evolves from $\mathcal{D}(t - dt, W)$ to $\mathcal{D}(t, W)$ at each time t , where dt represents the infinitesimal change in time.

Note that in the continuous tensor model, the modeled tensor changes ‘continuously’, i.e., once per minimum time unit in the input multi-aspect data stream (e.g., a millisecond), while the modeled tensor changes once per period T in the typical models, discussed in Section III.

B. Event-driven Implementation of Continuous Tensor Model

In the continuous tensor model, it is crucial to efficiently update the modeled tensor, or in other words, efficiently compute the change in $\mathcal{D}(t, W)$ in the modeled tensor. This is because repeatedly rebuilding the modeled tensor $\mathcal{D}(t, W)$ at every time t from scratch is computationally prohibitive.

We propose an efficient event-driven implementation of the continuous tensor model. Let $\mathcal{X} = \mathcal{D}(t, W)$ for simplicity. Our implementation, described in Algorithm 1, is based on the observation that each tuple $(e_n = (i_1, \dots, i_{M-1}, v_n), t_n)$ in the input multi-aspect data stream causes the following events:

- S.1** At time $t = t_n$, the value v_n is added to $x_{i_1, \dots, i_{M-1}, W}$.
- S.2** At time $t = t_n + wT$ for each $w \in \{1, \dots, W - 1\}$, the value v_n is subtracted from $x_{i_1, \dots, i_{M-1}, W-w+1}$ and then added to $x_{i_1, \dots, i_{M-1}, W-w}$.
- S.3** At time $t = t_n + WT$, the value v_n is subtracted from $x_{i_1, \dots, i_{M-1}, 1}$.

Algorithm 1: Event-driven Implementation of the Continuous Tensor Model

Input: (1) a multi-aspect data stream, (2) period T , (3) number of indices in the time mode W
Output: up-to-date tensor window $\mathcal{X} = \mathcal{D}(t, W)$
1 initialize \mathcal{X} to a zero tensor $\in \mathbb{R}^{N_1 \times \dots \times N_{M-1} \times W}$;
2 wait until an event E occurs ;
3 **if** $E = \text{arrival of } (e_n = (i_1, \dots, i_{M-1}, v_n), t_n)$ **then**
4 add v_n to $x_{i_1, \dots, i_{M-1}, W}$;
5 schedule the 1-st update for (e_n, t_n) at time $t_n + T$;
6 **if** $E = w\text{-th update for } (e_n = (i_1, \dots, i_{M-1}, v_n), t_n)$ **then**
7 subtract v_n from $x_{i_1, \dots, i_{M-1}, W-w+1}$;
8 **if** $w < W$ **then**
9 add v_n to $x_{i_1, \dots, i_{M-1}, W-w}$;
10 schedule the $(w + 1)$ -th update for (e_n, t_n) at time $t_n + (w + 1)T$;
11 **goto** Line 2

As formalized in Theorem 1, our implementation maintains the modeled tensor $\mathcal{X} = \mathcal{D}(t, W)$ up-to-date at each time t by performing $O(MW)$ operations per tuple in the input stream. Note that M and W are usually small numbers, and if we regard them as constants, the time complexity becomes $O(1)$, i.e. processing each tuple takes constant time.

Theorem 1 (Time Complexity of the Continuous Tensor Model). In Algorithm 1, the time complexity of processing each timestamped M -tuple is $O(MW)$.

Proof. For each timestamped M -tuple, $W + 1$ events occur. Processing an event (lines 4-5 or 7-10) takes $O(M)$ time. \square

Theorem 2 (Space Complexity of the Continuous Tensor Model). In Algorithm 1, the space complexity is

$$O\left(M \cdot \max_{t \in \mathbb{R}} |\{n \in \mathbb{N} : t_n \in (t - WT, t]\}|)\right).$$

Proof. We call $S_t \equiv \{n \in \mathbb{N} : t_n \in (t - WT, t]\}$ the set of active tuples at time t . The number of non-zeros in $\mathcal{X} = \mathcal{D}(t, W)$ is upper bounded by $|S_t|$, and thus the space required for \mathcal{X} is $O(M \cdot |S_t|)$. Since at most one event is scheduled for each active tuple, the space required for storing all scheduled events is also $O(M \cdot |S_t|)$. \square

V. PROPOSED OPTIMIZATION ALGORITHMS

In this section, we present the other part of SLICENSTITCH. We propose a family of online optimization algorithms for CPD of sparse tensors in the continuous tensor model. As stated in Problem 2, they aim to update factor matrices fast and accurately in response to each change in the tensor window.

Problem 2 (Online CP Decomposition of Sparse Tensors in the Continuous Tensor Model). **(1) Given:**

- the current tensor window $\mathcal{X} = \mathcal{D}(t, W)$,
- factor matrices $\mathbf{A}^{(1)}, \mathbf{A}^{(2)}, \dots, \mathbf{A}^{(M)}$ for \mathcal{X} ,
- an event for $(e_n = (i_1, \dots, i_{M-1}, v_n), t_n)$ occurring at t ,

(2) Update: the factor matrices in response to the event,

(3) To Solve: the minimization problem in Eq. (2).

Algorithm 2: SNS_{MAT}: Naive Extension of ALS.

- Input:** (1) current tensor window \mathcal{X} , (2) change $\Delta\mathcal{X}$,
(3) column-normalized factor matrices $\{\bar{\mathbf{A}}^{(m)}\}_{m=1}^M$,
(4) $\{\bar{\mathbf{A}}^{(m)'} \bar{\mathbf{A}}^{(m)}\}_{m=1}^M$

Output: Updated $\{\bar{\mathbf{A}}^{(m)}\}_{m=1}^M$, $\{\bar{\mathbf{A}}^{(m)'} \bar{\mathbf{A}}^{(m)}\}_{m=1}^M$, and λ

```

1 for  $m = 1, \dots, M$  do
2    $\mathbf{U} \leftarrow (\mathbf{X} + \Delta\mathbf{X})_{(m)} \left( \odot_{n \neq m}^M \bar{\mathbf{A}}^{(n)} \right)$ 
3    $\mathbf{H} \leftarrow *_{n \neq m}^M \bar{\mathbf{A}}^{(n)'} \bar{\mathbf{A}}^{(n)}$ 
4    $\mathbf{A}^{(m)} \leftarrow \mathbf{U} \mathbf{H}^\dagger$  // by Eq. (4)
5    $\lambda \leftarrow \ell^2$  norms of the columns of  $\mathbf{A}^{(m)}$  //  $\lambda \in \mathbb{R}^R$ 
6    $\bar{\mathbf{A}}^{(m)} \leftarrow$  column normalization of  $\mathbf{A}^{(m)}$ 
7   Update  $\bar{\mathbf{A}}^{(m)'} \bar{\mathbf{A}}^{(m)}$ 
8 return  $\{\bar{\mathbf{A}}^{(m)}\}_{m=1}^M$ ,  $\{\bar{\mathbf{A}}^{(m)'} \bar{\mathbf{A}}^{(m)}\}_{m=1}^M$ , and  $\lambda$ 

```

Below, we use $\Delta\mathcal{X}$ to denote the change in \mathcal{X} due to the given event. By S.1-S.3 of Section IV-B, Definition 6 follows.

Definition 6 (Input Change). The input change $\Delta\mathcal{X} \in \mathbb{R}^{N_1 \times \dots \times N_{M-1} \times W}$ is defined as the change in \mathcal{X} due to an event for $(e_n = (i_1, \dots, i_{M-1}, v_n), t_n)$ occurring at t , i.e.,

- [If $t = t_n$] The (i_1, \dots, i_{M-1}, W) -th entry of $\Delta\mathcal{X}$ is v_n , and the other entries are zero.
- [If $t = t_n + wT$ for $1 \leq w < W$] The $(i_1, \dots, i_{M-1}, W - w)$ -th and $(i_1, \dots, i_{M-1}, W - w + 1)$ -th entries of $\Delta\mathcal{X}$ are v_n and $-v_n$, respectively, and the others are zero.
- [If $t = t_n + WT$] The $(i_1, \dots, i_{M-1}, 1)$ -th entry of $\Delta\mathcal{X}$ is $-v_n$, and the others are zero.

We first introduce SLICENSTITCH-MATRIX (SNS_{MAT}), which naively applies ALS to Problem 2. Then, we present SLICENSTITCH-VECTOR (SNS_{VEC}) and SLICENSTITCH-RANDOM (SNS_{RND}). Lastly, we propose our main methods, SNS_{VEC}⁺ and SNS_{RND}⁺.

A. SLICENSTITCH-MATRIX (SNS_{MAT})

When we apply ALS to Problem 2, the factor matrices for the current window \mathcal{X} are strong initial points. Thus, a single iteration of ALS is enough to achieve high fitness. The detailed procedure of SNS_{MAT} is given in Algorithm 2. In line 6, we normalize¹ the columns of each updated factor matrices for balancing the scales of the factor matrices.

Pros and Cons: For each event, SNS_{MAT} accesses every entry of the current tensor window and updates every row of the factor matrices. Thus, it suffers from high computational cost, as formalized in Theorem 3, while it maintains a high-quality solution (i.e., factor matrices).

Theorem 3 (Time complexity of SNS_{MAT}). Let $N_M = W$. Then, the time complexity of SNS_{MAT} is

$$O\left(M^2 R |\mathcal{X} + \Delta\mathcal{X}| + M^2 R^2 + MR^3 + \sum_{m=1}^M N_m R^2\right). \quad (5)$$

Proof. See Section II.A of the online appendix [20]. \square

¹Let the r -th entry of $\lambda \in \mathbb{R}^R$ as λ_r , and the r -th column of $\mathbf{A}^{(m)}$ be $\mathbf{a}_r^{(m)}$. We set λ_r to $\|\mathbf{a}_r^{(m)}\|_2$ and set $\bar{\mathbf{a}}_r^{(m)}$ to $\mathbf{a}_r^{(m)}/\lambda_r$ for $r = 1, \dots, R$. Then, \mathcal{X} is approximated as $\sum_{r=1}^R \lambda_r \bar{\mathbf{a}}_r^{(1)} \circ \bar{\mathbf{a}}_r^{(2)} \circ \dots \circ \bar{\mathbf{a}}_r^{(M)}$.

Algorithm 3: Common Outline of SNS_{VEC}, SNS_{VEC}⁺, SNS_{RND}, and SNS_{RND}⁺.

- Input:** (1) current tensor window $\mathcal{X} = \mathcal{D}(t, W)$,
(2) change $\Delta\mathcal{X}$ due to an event for
 $(e_n = (i_1, \dots, i_{M-1}, v_n), t_n)$ occurring at t ,
(3) factor matrices $\{\mathbf{A}^{(m)}\}_{m=1}^M$
(4) $\{\mathbf{A}^{(m)'} \mathbf{A}^{(m)}\}_{m=1}^M$, (5) period T

Output: updated $\{\mathbf{A}^{(m)}\}_{m=1}^M$ and $\{\mathbf{A}^{(m)'} \mathbf{A}^{(m)}\}_{m=1}^M$

```

1  $\{\mathbf{A}_{prev}^{(m)'} \mathbf{A}^{(m)}\}_{m=1}^M \leftarrow \{\mathbf{A}^{(m)'} \mathbf{A}^{(m)}\}_{m=1}^M$  // used only
   in SNSRND and SNSRND+
2  $w \leftarrow (t - t_n)/T$  // time-mode index
3 if  $w > 0$  then
4   updateRow( $M, W - w + 1, \dots$ ) // Alg. 4 or 5
5 if  $w < W$  then
6   updateRow( $M, W - w, \dots$ ) // Alg. 4 or 5
7 for  $m \leftarrow 1, \dots, M - 1$  do
8   updateRow( $m, i_m$ ) // Alg. 4 or 5
9 return  $\{\mathbf{A}^{(m)}\}_{m=1}^M$  and  $\{\mathbf{A}^{(m)'} \mathbf{A}^{(m)}\}_{m=1}^M$ 

```

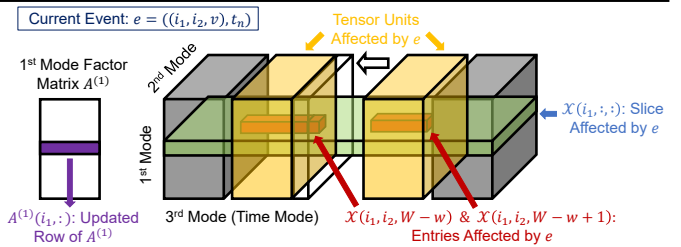


Fig. 3. **Example: updating a row of $\mathbf{A}^{(1)}$.** SNS_{VEC} and SNS_{RND} update $\mathbf{A}^{(1)}(i_1, :)$ at once. SNS_{VEC}⁺ and SNS_{RND}⁺ update it entry by entry. SNS_{RND} and SNS_{RND}⁺ sample θ entries from those in $\mathcal{X}(i_1, :, :)$ if more than θ entries there are non-zero (i.e., if $\text{deg}(1, i_1) > \theta$).

B. SLICENSTITCH-VECTOR (SNS_{VEC})

We propose SNS_{VEC}, a fast algorithm for Problem 2. The outline of SNS_{VEC} is given in Algorithm 3, and the update rules are given in Algorithm 4 with a running example in Fig. 3. The key idea of SNS_{VEC} is to update only the rows of factor matrices that approximate changed entries of the tensor window. Starting from the maintained factor matrices, SNS_{VEC} updates such rows of the time-mode factor matrix (lines 3-6) and then such rows of the non-time mode factor matrices (lines 7-8). Below, we describe the update rules used.

Time Mode: Real-world tensors are typically modeled so that the time mode of \mathcal{X} has fewer indices than the other modes. Thus, each tensor unit (see Definition 3) in \mathcal{X} is likely to contain many non-zeros, and thus even updating only few rows of the time-mode factor matrix (i.e., $\mathbf{A}^{(M)}$) is likely to incur considerable computational cost. To avoid the cost, SNS_{VEC} employs an approximated update rule.

From Eq. (4), the following update rule for the time-mode factor matrix follows:

$$\mathbf{A}^{(M)} \leftarrow (\mathbf{X} + \Delta\mathbf{X})_{(M)} \mathbf{K}^{(M)} \mathbf{H}^{(M)\dagger}, \quad (6)$$

where $\mathbf{K}^{(M)} = \odot_{m=1}^{M-1} \mathbf{A}^{(m)}$ and $\mathbf{H}^{(M)} = *_{m=1}^{M-1} \mathbf{A}^{(m)'} \mathbf{A}^{(m)}$. If we assume that the approximated tensor \mathcal{X} in Eq. (1) approximates \mathcal{X} well, then Eq. (6) is approximated to Eq. (7).

$$\mathbf{A}^{(M)} \leftarrow \mathbf{A}^{(M)} \mathbf{K}^{(M)'} \mathbf{K}^{(M)} \mathbf{H}^{(M)\dagger} + \Delta\mathbf{X}_{(M)} \mathbf{K}^{(M)} \mathbf{H}^{(M)\dagger}. \quad (7)$$

By a property of the Khatri-Rao product [19], Eq. (8) holds.

$$\begin{aligned} \mathbf{K}^{(M)'} \mathbf{K}^{(M)} &= \left(\odot_{m=1}^{M-1} \mathbf{A}^{(m)} \right)' \left(\odot_{m=1}^{M-1} \mathbf{A}^{(m)} \right) \\ &= *_{m=1}^{M-1} \mathbf{A}^{(m)'} \mathbf{A}^{(m)} = \mathbf{H}^{(M)}. \end{aligned} \quad (8)$$

By Eq. (8), Eq. (7) is reduced to Eq. (9).

$$\mathbf{A}^{(M)} \leftarrow \mathbf{A}^{(M)} + \Delta \mathbf{X}_{(M)} \mathbf{K}^{(M)} \mathbf{H}^{(M)\dagger}. \quad (9)$$

Computing Eq. (9) is much cheaper than computing Eq. (6). Since $\Delta \mathbf{X}_{(M)}$ contains at most two non-zeros (see Problem 2), computing $\Delta \mathbf{X}_{(M)} \mathbf{K}^{(M)}$ in Eq. (9) takes $O(MR)$ time. Due to the same reason, at most two rows of $\mathbf{A}^{(M)}$ are updated.

Non-time Modes: When updating $\mathbf{A}^{(m)}$, while fixing the other factor matrices, the objective Eq. (3) becomes Eq. (10).

$$\min_{\mathbf{A}^{(m)}} \left\| (\mathbf{X} + \Delta \mathbf{X})_{(m)} - \mathbf{A}^{(m)} \left(\odot_{n \neq m}^M \mathbf{A}^{(n)} \right)' \right\|_F. \quad (10)$$

Note that $\Delta \mathbf{X}$ contains up to two non-zeros, which are the entries changed in \mathcal{X} , and their m -th mode indices are i_m (see Problem 2). By Eq. (3), only the i_m -th row of $\mathbf{A}^{(m)}$ is used to approximate the changed entries, and thus SNS_{VEC} updates only the row.

If we fix all the other variables except $\mathbf{A}^{(m)}(i_m, :)$, the problem in Eq. (10) becomes the problem in Eq. (11).

$$\begin{aligned} \min_{\mathbf{A}^{(m)}(i_m, :)} \left\| (\mathbf{X} + \Delta \mathbf{X})_{(m)}(i_m, :) \right. \\ \left. - \mathbf{A}^{(m)}(i_m, :) \left(\odot_{n \neq m}^M \mathbf{A}^{(n)} \right)' \right\|_F. \end{aligned} \quad (11)$$

The problem in Eq. (11) is a least-square problem, and its analytical solution in Eq. (12) is available.

$$\mathbf{A}^{(m)}(i_m, :) \leftarrow (\mathbf{X} + \Delta \mathbf{X})_{(m)}(i_m, :) \mathbf{K}^{(m)} \mathbf{H}^{(m)\dagger}, \quad (12)$$

where $\mathbf{K}^{(m)} = \odot_{n \neq m}^M \mathbf{A}^{(n)}$ and $\mathbf{H}^{(m)} = *_{n \neq m}^M \mathbf{A}^{(n)'} \mathbf{A}^{(n)}$.

After updating the i_m -th row of each m -th mode factor matrix $\mathbf{A}^{(m)}$ either by Eq. (9) or Eq. (12), SNS_{VEC} incrementally maintains $\mathbf{A}^{(m)'} \mathbf{A}^{(m)}$ up to date by Eq. (13).

$$\mathbf{A}^{(m)'} \mathbf{A}^{(m)} \leftarrow \mathbf{A}^{(m)'} \mathbf{A}^{(m)} - \mathbf{p}' \mathbf{p} + \mathbf{A}^{(m)}(i_m, :)' \mathbf{A}^{(m)}(i_m, :), \quad (13)$$

where \mathbf{p} is the i_m -th row of $\mathbf{A}^{(m)}$ before the update.

Pros and Cons: By updating only few rows of each factor matrix, SNS_{VEC} significantly reduces the computational cost of SNS_{MAT} , as formalized in Theorem 4, without much loss in the quality of the solution. However, SNS_{VEC} slows down if many non-zeros are of the same index (see Eq. (14)), and it is often unstable due to round errors, as discussed later.

Theorem 4 (Time complexity of SNS_{VEC}). Let $\text{deg}(m, i_m) \equiv |(\mathbf{X} + \Delta \mathbf{X})_{(m)}(i_m, :)|$ be the number of non-zeros of $\mathbf{X} + \Delta \mathbf{X}$ whose m -th mode index is i_m . Then, the time complexity of SNS_{VEC} is

$$O\left(MR \sum_{m=1}^{M-1} \text{deg}(m, i_m) + (MR)^2 + MR^3\right). \quad (14)$$

Proof. See Section II.B of the online appendix [20]. \square

Algorithm 4: updateRow in SNS_{VEC} and SNS_{RND}

// Parenthesized inputs/outputs are for SNS_{RND}

Input: (1) mode m and index i_m to be updated
 (2) current tensor window \mathcal{X} , (3) change $\Delta \mathcal{X}$,
 (4) factor matrices $\{\mathbf{A}^{(m)}\}_{m=1}^M$ for \mathcal{X} ,
 (5) $\{\mathbf{A}^{(m)'} \mathbf{A}^{(m)}\}_{m=1}^M$ (and $\{\mathbf{A}_{\text{prev}}^{(m)'} \mathbf{A}^{(m)}\}_{m=1}^M$),
 (6) (threshold θ for sampling)

Output: updated $\mathbf{A}^{(m)}$, $\mathbf{A}^{(m)'} \mathbf{A}^{(m)}$ (and $\mathbf{A}_{\text{prev}}^{(m)'} \mathbf{A}^{(m)}$)

// updateRow implemented in SNS_{VEC}

1 **Procedure** updateRowVec(m, i_m, \dots):

2 $\mathbf{p} \leftarrow \mathbf{A}^{(m)}(i_m, :)$
 3 **if** $m = M$ **then** Update $\mathbf{A}^{(m)}(i_m, :)$ by Eq. (9)
 4 **else** Update $\mathbf{A}^{(m)}(i_m, :)$ by Eq. (12)
 5 Update $\mathbf{A}^{(m)'} \mathbf{A}^{(m)}$ by Eq. (13)
 6 **return** $\mathbf{A}^{(m)}$ and $\mathbf{A}^{(m)'} \mathbf{A}^{(m)}$

// updateRow implemented in SNS_{RND}

7 **Procedure** updateRowRan(m, i_m, \dots):

8 $\mathbf{p} \leftarrow \mathbf{A}^{(m)}(i_m, :)$
 9 **if** $\text{deg}(m, i_m) \leq \theta$ **then**
 10 Update $\mathbf{A}^{(m)}(i_m, :)$ by Eq. (12)
 11 **else**
 12 $S \leftarrow \theta$ indices of \mathcal{X} chosen uniformly at random,
 while fixing the m -th mode index to i_m
 13 Compute $\tilde{\mathcal{X}}$ from S
 14 Update $\mathbf{A}^{(m)}(i_m, :)$ by Eq. (16)
 15 Update $\mathbf{A}^{(m)'} \mathbf{A}^{(m)}$ by Eq. (13)
 16 Update $\mathbf{A}_{\text{prev}}^{(m)'} \mathbf{A}^{(m)}$ by Eq. (17)
 17 **return** $\mathbf{A}^{(m)}$, $\mathbf{A}^{(m)'} \mathbf{A}^{(m)}$, and $\mathbf{A}_{\text{prev}}^{(m)'} \mathbf{A}^{(m)}$

C. SLICENSTITCH-RANDOM (SNS_{RND})

We introduce SNS_{RND} , which is even faster than SNS_{VEC} . The outline of SNS_{RND} (see Algorithm 3) is the same with that of SNS_{VEC} . That is, SNS_{RND} also updates only the rows of the factor matrices that approximate the changed entries in the current tensor window \mathcal{X} . However, when updating such a row, the number of entries accessed by SNS_{RND} is upper bounded by a user-specific constant θ , while SNS_{VEC} accesses $\text{deg}(m, i_m)$ entries (see Theorem 4), which can be as many as all the entries in \mathcal{X} . Below, we present its update rule.

Assume SNS_{RND} updates the i_m -th row of $\mathbf{A}^{(m)}$. That is, consider the problem in Eq. (11). As described in the procedure updateRowRan in Algorithm 4, SNS_{RND} uses different approaches depending on a user-specific threshold θ and $\text{deg}(m, i_m) \equiv |(\mathbf{X} + \Delta \mathbf{X})_{(m)}(i_m, :)|$, i.e., the number of non-zeros of $\mathcal{X} + \Delta \mathcal{X}$ whose M -th mode index is i_m . If $\text{deg}(m, i_m)$ is smaller than or equal to θ , then SNS_{RND} uses Eq. (12) (lines 9-10), which is also used in SNS_{VEC} .

However, if $\text{deg}(m, i_m)$ is greater than θ , SNS_{RND} speeds up the update through approximation. First, it samples θ indices from \mathcal{X} without replacement, while fixing the M -th mode index to i_m (line 12).² Let the set of sampled indices be S , and let $\tilde{\mathcal{X}} \in \mathbb{R}^{N_1 \times \dots \times N_{M-1} \times W}$ be a tensor whose entries are all 0 except those with the sampled indices S . For each sampled index $J = (j_1, \dots, j_M) \in S$, $\tilde{x}_J = x_J - \tilde{x}_J$. Note that for any index $J = (j_1, \dots, j_M)$ of \mathcal{X} , $\tilde{x}_J + \tilde{x}_J = x_J$ if $J \in S$

²We ignore the indices of non-zeros in $\Delta \mathcal{X}$ even if they are sampled.

and $\tilde{x}_J + \bar{x}_J = \tilde{x}_J$ otherwise. Thus, the more samples SNS_{RND} draws with larger S , the closer $\tilde{\mathcal{X}} + \bar{\mathcal{X}}$ is to \mathcal{X} . SNS_{RND} uses $\tilde{\mathcal{X}} + \bar{\mathcal{X}}$ to approximate \mathcal{X} in the update. Specifically, it replaces \mathcal{X} of the objective function in Eq. (11) with $\tilde{\mathcal{X}} + \bar{\mathcal{X}}$. Then, as in Eq. (12), the update rule in Eq. (15) follows.

$$\mathbf{A}^{(m)}(i_m, :) \leftarrow (\tilde{\mathcal{X}} + \bar{\mathcal{X}} + \Delta\mathcal{X})_{(m)}(i_m, :) \mathbf{K}^{(m)} \mathbf{H}^{(m)\dagger}, \quad (15)$$

where $\mathbf{K}^{(m)} = \odot_{n \neq m}^M \mathbf{A}^{(n)}$ and $\mathbf{H}^{(m)} = *_{n \neq m}^M \mathbf{A}^{(n)'} \mathbf{A}^{(n)}$. Let $\mathbf{A}_{\text{prev}}^{(m)}$ be the m -th mode factor matrix before the update and $\mathbf{H}_{\text{prev}}^{(m)}$ be $*_{n \neq m}^M \mathbf{A}_{\text{prev}}^{(n)'} \mathbf{A}_{\text{prev}}^{(n)}$. By Eq. (8), Eq. (15) is equivalent to Eq. (16).

$$\mathbf{A}^{(m)}(i_m, :) \leftarrow \mathbf{A}^{(m)}(i_m, :) \mathbf{H}_{\text{prev}}^{(m)} \mathbf{H}^{(m)\dagger} + (\bar{\mathcal{X}} + \Delta\mathcal{X})_{(m)} \mathbf{K}^{(m)} \mathbf{H}^{(m)\dagger}. \quad (16)$$

Noteworthy, $(\bar{\mathcal{X}} + \Delta\mathcal{X})_{(m)}$ has at most $\theta + 2 = O(\theta)$ non-zeros. SNS_{RND} uses Eq. (16) to update the i_m -th row of $\mathbf{A}^{(m)}$ (line 14 of Algorithm 4). It incrementally maintains $\mathbf{A}^{(m)'} \mathbf{A}^{(m)}$ up to date by Eq. (13) (line 15), as SNS_{VEC} does. It also maintains $\mathbf{A}_{\text{prev}}^{(m)'} \mathbf{A}^{(m)}$ up to date by Eq. (17) (line 16).

$$\mathbf{A}_{\text{prev}}^{(m)'} \mathbf{A}^{(m)} \leftarrow \mathbf{A}_{\text{prev}}^{(m)'} \mathbf{A}^{(m)} - \mathbf{p}' \mathbf{p} + \mathbf{p}' \mathbf{A}^{(m)}(i_m, :), \quad (17)$$

where $\mathbf{p} = \mathbf{A}_{\text{prev}}^{(m)}(i_m, :)$.

Pros and Cons: Through approximation, SNS_{RND} upper bounds the number of non-zeros of $(\bar{\mathcal{X}} + \Delta\mathcal{X})_{(m)}$ in Eq. (16) by $O(\theta)$. As a result, the time complexity of SNS_{RND} , given in Theorem 5, is lower than that of SNS_{VEC} . Specifically, $\text{deg}(m, i_m)$ in Eq. (14), which can be as big as $|\mathcal{X} + \Delta\mathcal{X}|$, is replaced with the user-specific constant θ in Eq. (18). Noteworthy, if we regard M , R , and θ in Eq. (18) as constants, **the time complexity of SNS_{RND} becomes constant**. This change makes SNS_{RND} significantly faster than SNS_{VEC} , at the expense of a slight reduction in the quality of the solution.

Theorem 5 (Time complexity of SNS_{RND}). If $\theta > 1$, then the time complexity of SNS_{RND} is

$$O\left(M^2 R \theta + M^2 R^2 + M R^3\right). \quad (18)$$

If M , R , and θ are regarded as constants, Eq. (18) is $O(1)$.

Proof. See Section II.C of the online appendix [20]. \square

Unlike SNS_{MAT} , SNS_{VEC} and SNS_{RND} do not normalize the columns of factor matrices during the update process. This is because normalization requires $O(R \sum_{m=1}^M N_m)$ time, which is proportional to the number of all entries in all factor matrices, and thus significantly increases the time complexity of SNS_{VEC} and SNS_{RND} . However, without normalization, the entries of factor matrices may have extremely large or extremely small absolute values, making SNS_{VEC} and SNS_{RND} vulnerable to numerical errors. In our experiments (see Fig. 4 in Section VI-C), the accuracies of SNS_{VEC} and SNS_{RND} suddenly drop due to numerical errors in some datasets.

D. SLICENSTITCH-STABLE ($\text{SNS}_{\text{VEC}}^+$ and $\text{SNS}_{\text{RND}}^+$)

In this section, we propose $\text{SNS}_{\text{VEC}}^+$ and $\text{SNS}_{\text{RND}}^+$, which successfully address the aforementioned instability of SNS_{VEC} and SNS_{RND} . The main idea is to clip each entry, (i.e., ensure that each entry is within a predefined range), while at the same time ensuring that the objective function does not increase. To this end, $\text{SNS}_{\text{VEC}}^+$ and $\text{SNS}_{\text{RND}}^+$ employs coordinate descent, where each entry of factor matrices is updated one by one. The outline of $\text{SNS}_{\text{VEC}}^+$ and $\text{SNS}_{\text{RND}}^+$ (see Algorithm 3) is the same as that of SNS_{VEC} and SNS_{RND} . Below, we present their update rules, which are used in Algorithm 5.

Coordinate descent updates one variable (i.e., entry of a factor matrix) at a time while fixing all the other variables. Assume an entry $a_{i_m k}^{(m)}$ of $\mathbf{A}^{(m)}$ is updated. Solving the problem in Eq. (2) with respect to $a_{i_m k}^{(m)}$ while fixing the other variables is equivalent to solving the problem in Eq. (19).

$$\min_{a_{i_m k}^{(m)}} \sum_{J \in \Omega_{i_m}^{(m)}} (x_J + \Delta x_J - \sum_{r \neq k}^R \prod_{n=1}^M a_{j_n r}^{(n)} - a_{i_m k}^{(m)} \prod_{n \neq m}^M a_{j_n k}^{(n)})^2, \quad (19)$$

where $J = (j_1, \dots, j_M)$, and $\Omega_{i_m}^{(m)}$ is the set of indices of \mathcal{X} of which the m -th mode index is i_m . To describe its solution, we first define the following terms:

$$\begin{aligned} c_k^{(m)} &\equiv \prod_{n \neq m}^M \left(\sum_{j_n=1}^{N_n} (a_{j_n k}^{(n)})^2 \right), \\ d_{i_m k}^{(m)} &\equiv \sum_{r \neq k}^R \left(a_{i_m r}^{(m)} \prod_{n \neq m}^M \left(\sum_{j_n=1}^{N_n} a_{j_n r}^{(n)} a_{j_n k}^{(n)} \right) \right), \\ e_{i_m k}^{(m)} &\equiv \sum_{r=1}^R \left(b_{i_m r}^{(m)} \prod_{n \neq m}^M \left(\sum_{j_n=1}^{N_n} b_{j_n r}^{(n)} a_{j_n k}^{(n)} \right) \right), \end{aligned} \quad (20)$$

where $\mathbf{B}^{(m)} \equiv \mathbf{A}_{\text{prev}}^{(m)}$ is $\mathbf{A}^{(m)}$ before any update.

Solving the Problem in Eq. (19): The problem in Eq. (19) is a least square problem, and thus there exists the closed-form solution, which is used to update $a_{i_m k}^{(m)}$ in Eq. (21).

$$a_{i_m k}^{(m)} \leftarrow \left(\sum_{J \in \Omega_{i_m}^{(m)}} ((x_J + \Delta x_J) \prod_{n \neq m}^M a_{j_n k}^{(n)}) - d_{i_m k}^{(m)} \right) / c_k^{(m)}. \quad (21)$$

Eq. (21) is used, instead of Eq. (12), when updating non-time mode factor matrices (i.e., when $m \neq M$) in $\text{SNS}_{\text{VEC}}^+$ (line 4 of Algorithm 5). It is also used, instead of Eq. (12), in $\text{SNS}_{\text{RND}}^+$ when $\text{deg}(m, i_m) \leq \theta$ (line 13). As in SNS_{VEC} , when updating the time-mode factor matrix, $\text{SNS}_{\text{VEC}}^+$ approximates \mathcal{X} by $\tilde{\mathcal{X}}$, and thus it uses Eq. (22) (line 3).

$$a_{i_m k}^{(m)} \leftarrow \left(e_{i_m k}^{(m)} + \sum_{J \in \Omega_{i_m}^{(m)}} (\Delta x_J \prod_{n \neq m}^M a_{j_n k}^{(n)}) - d_{i_m k}^{(m)} \right) / c_k^{(m)}. \quad (22)$$

Similarly, as in SNS_{RND} , when $\text{deg}(m, i_m) > \theta$, $\text{SNS}_{\text{RND}}^+$ approximates \mathcal{X} by $\tilde{\mathcal{X}} + \bar{\mathcal{X}}$, and thus it uses Eq. (23) (line 14).

$$a_{i_m k}^{(m)} \leftarrow \left(e_{i_m k}^{(m)} + \sum_{J \in \Omega_{i_m}^{(m)}} ((\tilde{x}_J + \Delta x_J) \prod_{n \neq m}^M a_{j_n k}^{(n)}) - d_{i_m k}^{(m)} \right) / c_k^{(m)}. \quad (23)$$

Note that all Eq. (21), Eq. (22), and Eq. (23) are based on Eq. (20). For the rapid computation of Eq. (20), $\text{SNS}^+_{\text{VEC}}$ and $\text{SNS}^+_{\text{RND}}$ incrementally maintain $\sum_{j_m=1}^{N_m} (a_{j_m k}^{(m)})^2$ and $\sum_{j_m=1}^{N_m} a_{j_m r}^{(m)} a_{j_m k}^{(m)}$, which are the (k, k) -th and (r, k) -th entries of $\mathbf{A}^{(m)} \mathbf{A}^{(m)}$, by Eq. (24) and Eq. (25) (lines 6 and 16). $\text{SNS}^+_{\text{RND}}$ also incrementally maintains $\sum_{j_m=1}^{N_m} b_{j_m r}^{(m)} a_{j_m k}^{(m)}$, which is the (r, k) -th entry of $\mathbf{A}_{\text{prev}}^{(m)'} \mathbf{A}^{(m)}$, by Eq. (26) (line 17).

$$q_{kk}^{(m)} \leftarrow q_{kk}^{(m)} - (b_{i_m k}^{(m)})^2 + (a_{i_m k}^{(m)})^2, \quad (24)$$

$$q_{rk}^{(m)} \leftarrow q_{rk}^{(m)} - a_{i_m r}^{(m)} b_{i_m k}^{(m)} + a_{i_m r}^{(m)} a_{i_m k}^{(m)}, \quad (25)$$

$$u_{rk}^{(m)} \leftarrow u_{rk}^{(m)} - b_{i_m r}^{(m)} b_{i_m k}^{(m)} + b_{i_m r}^{(m)} a_{i_m k}^{(m)}, \quad (26)$$

where $\mathbf{Q}^{(m)} \equiv \mathbf{A}^{(m)'} \mathbf{A}^{(m)}$ and $\mathbf{U}^{(m)} \equiv \mathbf{A}_{\text{prev}}^{(m)'} \mathbf{A}^{(m)}$. Proofs of Eqs. (21)-(26) can be found in an online appendix [20].

Clipping: In order to prevent the entries of factor matrices from having extremely large or small absolute values, $\text{SNS}^+_{\text{VEC}}$ and $\text{SNS}^+_{\text{RND}}$ ensures that its absolute value is at most η , which is a user-specific threshold. Specifically, if the updated entry is greater than η , it is set to η , and if the updated entry is smaller than $-\eta$, it is set to $-\eta$ (lines 5 and 15 in Algorithm 5). Eq. (21) followed by clipping never increases the objective function in Eq. (19).^{3,4}

Pros and Cons: $\text{SNS}^+_{\text{VEC}}$ and $\text{SNS}^+_{\text{RND}}$ does not suffer from instability due to numerical errors, which SNS_{VEC} and SNS_{RND} suffer from. Moreover, as shown in Theorems 6 and 7, the time complexities of $\text{SNS}^+_{\text{VEC}}$ and $\text{SNS}^+_{\text{RND}}$ are lower than those of SNS_{VEC} and SNS_{RND} , respectively. Empirically, however, $\text{SNS}^+_{\text{VEC}}$ and $\text{SNS}^+_{\text{RND}}$ are slightly slower and less accurate than SNS_{VEC} and SNS_{RND} , respectively (see Section VI-C).

Theorem 6 (Time complexity of $\text{SNS}^+_{\text{VEC}}$). The time complexity of $\text{SNS}^+_{\text{VEC}}$ is

$$O\left(MR \sum_{m=1}^{M-1} \text{deg}(m, i_m) + M^2 R^2\right). \quad (27)$$

Proof. See Section II.E of the online appendix [20]. \square

Theorem 7 (Time complexity of $\text{SNS}^+_{\text{RND}}$). If $\theta > 1$, then the time complexity of $\text{SNS}^+_{\text{RND}}$ is

$$O\left(M^2 R \theta + M^2 R^2\right). \quad (28)$$

If M , R , and θ are regarded as constants, Eq. (28) is $O(1)$.

Proof. See Section II.F of the online appendix [20]. \square

VI. EXPERIMENTS

In this section, we design and review experiments to answer the following questions:

- **Q1. Advantages of Continuous CP Decomposition:** What are the advantages of continuous CP decomposition over conventional CP decomposition?

³Let x , y , and z be $a_{i_m k}^{(m)}$ before update, after being updated by Eq. (21), and after being clipped, respectively. The objective function in Eq. (19) is convex, minimized at y , and symmetric around y . $|y - z| \leq |y - x|$ holds.

⁴For Eq. (22) and Eq. (23), this is true only when \mathcal{X} is well approximated.

Algorithm 5: updateRow in $\text{SNS}^+_{\text{VEC}}$ and $\text{SNS}^+_{\text{RND}}$

```
// Parenthesized inputs/outputs are for  $\text{SNS}^+_{\text{RND}}$ 
Input: (1) mode  $m$  and index  $i_m$  to be updated,
        (2) current tensor window  $\mathcal{X}$ , (3) change  $\Delta \mathcal{X}$ ,
        (4) factor matrices  $\{\mathbf{A}^{(m)}\}_{m=1}^M$  for  $\mathcal{X}$ 
        (5)  $\{\mathbf{A}^{(m)'} \mathbf{A}^{(m)}\}_{m=1}^M$  (and  $\{\mathbf{A}_{\text{prev}}^{(m)'} \mathbf{A}^{(m)}\}_{m=1}^M$ )
        (6)  $\eta$  for clipping (and threshold  $\theta$  for sampling)
Output: updated  $\mathbf{A}^{(m)}$ ,  $\mathbf{A}^{(m)'} \mathbf{A}^{(m)}$  (and  $\mathbf{A}_{\text{prev}}^{(m)'} \mathbf{A}^{(m)}$ )
// updateRow implemented in  $\text{SNS}^+_{\text{VEC}}$ 
1 Procedure updateRowVec+ ( $m, i_m, \dots$ ):
2   for  $k = 1, \dots, R$  do
3     if  $m = M$  then Update  $a_{i_m k}^{(m)}$  by Eq. (22)
4     else Update  $a_{i_m k}^{(m)}$  by Eq. (21)
5     if  $|a_{i_m k}^{(m)}| > \eta$  then  $a_{i_m k}^{(m)} \leftarrow \text{sign}(a_{i_m k}^{(m)}) \cdot \eta$ 
6     Update  $\mathbf{A}^{(m)'} \mathbf{A}^{(m)}$  by Eq. (24) and Eq. (25)
7   return  $\mathbf{A}^{(m)}$  and  $\mathbf{A}^{(m)'} \mathbf{A}^{(m)}$ 
// updateRow implemented in  $\text{SNS}^+_{\text{RND}}$ 
8 Procedure updateRowRan+ ( $m, i_m, \dots$ ):
9   if  $\text{deg}(m, i_m) > \theta$  then
10     $S \leftarrow \theta$  indices of  $\mathcal{X}$  chosen uniformly at random,
11    while fixing the  $m$ -th mode index to  $i_m$ 
12    Compute  $\tilde{\mathcal{X}}$  from  $S$ 
13  for  $k = 1, \dots, R$  do
14    if  $\text{deg}(m, i_m) \leq \theta$  then Update  $a_{i_m k}^{(m)}$  by Eq. (21)
15    else Update  $a_{i_m k}^{(m)}$  by Eq. (23)
16    if  $|a_{i_m k}^{(m)}| > \eta$  then  $a_{i_m k}^{(m)} \leftarrow \text{sign}(a_{i_m k}^{(m)}) \cdot \eta$ 
17    Update  $\mathbf{A}^{(m)'} \mathbf{A}^{(m)}$  by Eq. (24) and Eq. (25)
18    Update  $\mathbf{A}_{\text{prev}}^{(m)'} \mathbf{A}^{(m)}$  by Eq. (26)
19  return  $\mathbf{A}^{(m)}$ ,  $\mathbf{A}^{(m)'} \mathbf{A}^{(m)}$ , and  $\mathbf{A}_{\text{prev}}^{(m)'} \mathbf{A}^{(m)}$ 
```

- **Q2. Speed and Fitness:** How rapidly and precisely does SLICENSTITCH fit the input tensor, compared to baselines?
- **Q3. Data Scalability:** How does SLICENSTITCH scale with regard to the number of events?
- **Q4. Effect of Parameters:** How do user-specific thresholds θ and η affect the performance of SLICENSTITCH?
- **Q5. Practitioner's Guide:** Which versions of SLICENSTITCH do we have to use?
- **Q6. Application to Anomaly Detection:** Can SLICENSTITCH spot abnormal events rapidly and accurately?

A. Experiment Specifications

Machine: We ran all experiments on a machine with a 3.7GHz Intel i5-9600K CPU and 64GB memory.

Datasets: We used four different real-world sparse tensor datasets summarized in Table II. They are sparse tensors with a time mode, and their densities vary from 10^{-2} to 10^{-6} .

Evaluation Metrics: We evaluated SLICENSTITCH and baselines using the following metrics:

- **Elapsed Time per Update:** The average elapsed time for updating the factor matrices in response to each event.
- **Fitness** (The higher the better): *Fitness* is a widely-used metric to evaluate the accuracy of tensor decomposition algorithms. It is defined as $1 - (\|\tilde{\mathcal{X}} - \mathcal{X}\|_F / \|\mathcal{X}\|_F)$, where \mathcal{X} is the input tensor, and $\tilde{\mathcal{X}}$ (Eq. (1)) is its approximation.

TABLE II

SUMMARY OF REAL-WORLD SPARSE TENSOR DATASETS. ALL LINKS ARE AT [HTTPS://GITHUB.COM/DMLAB-TENSOR/SLICENSTITCH#DATASETS](https://github.com/DMLAB-TENSOR/SLICENSTITCH#DATASETS).

Name	Description	Size	# Non-zeros	Density
Divvy Bikes	sources \times destinations \times timestamps [minutes]	$673 \times 673 \times 525594$	3.82M	1.604×10^{-5}
Chicago Crime	communities \times crime types \times timestamps [hours]	$77 \times 32 \times 148464$	5.33M	1.457×10^{-2}
New York Taxi	sources \times destinations \times timestamps [seconds]	$265 \times 265 \times 5184000$	84.39M	2.318×10^{-4}
Ride Austin	sources \times destinations \times colors \times timestamps [minutes]	$219 \times 219 \times 24 \times 285136$	0.89M	2.739×10^{-6}

- **Relative Fitness** [16] (The higher the better): *Relative fitness*, which is defined as the ratio between the fitness of the target algorithm and the fitness of ALS, i.e.,

$$\text{Relative Fitness} \equiv \frac{\text{Fitness}_{\text{target}}}{\text{Fitness}_{\text{ALS}}}$$

Recall that ALS (see Section II) is the standard batch algorithm for tensor decomposition.

Baselines: Since there is no previous algorithm for continuous CPD, we compared SLICENSTITCH with ALS, OnlineSCP [16], CP-stream [15], and NeCPD (n) with n iterations [28], all of which are for conventional CPD (see Section VII). All baselines except ALS update factor matrices once per period T (instead of whenever an event occurs).⁵ We implemented SLICENSTITCH and ALS in C++. We used the official implementation of OnlineSCP in MATLAB and that of CP-stream in C++.⁶ We implemented NeCPD in MATLAB.

Experimental Setup: We set the hyperparameters as listed in Table III unless otherwise stated. We set the threshold θ for sampling to be smaller than half of the average degree of indices (i.e., the average number of non-zeros when fixing an index) in the initial tensor window. In each experiment, we initialized factor matrices using ALS on the initial tensor window, and we processed the events during $5WT$ time units. We measured relative fitness 5 times.

B. Q1. Advantages of Continuous CP Decomposition

We compared the continuous CPD and conventional CPD, in terms of the update interval (i.e., the minimum interval between two consecutive updates), fitness, and the number of parameters, using the New York Taxi dataset. We used SNS_{RND} and fixed the period T to 1 hour for continuous CPD; and we used CP-stream, OnlineSCP, and ALS while varying T (i.e., the granularity of the time mode) from 1 second to 1 hour for conventional CPD. Fig. 1 shows the result,⁷ and we found Observation 1.

Observation 1 (Advantages of Continuous CPD). Continuous CPD achieved (a) near-instant updates, (b) high fitness, and (c) a small number of parameters at the same time, while conventional CPD cannot. When the update interval was the same, continuous CPD achieved **2.26 \times higher fitness with 55 \times fewer parameters** than conventional CPD. When they showed similar fitness, the update interval of continuous CPD was **3600 \times shorter** than that of conventional CPD.

⁵We modified the baselines, which are for decomposing the entire tensor, to decompose the tensor window (see Definition 4), as SLICENSTITCH does.

⁶<https://shuozhou.github.io>, <https://github.com/ShadenSmith/splatt-stream>

⁷Before measuring the fitness of all baselines, we merged the rows of fine-grained time-mode factor matrices sequentially by adding entries so that one row corresponds to an hour. Without this postprocessing step, the fitness of the baselines was even lower than those reported in Fig. 1c.

TABLE III
DEFAULT HYPERPARAMETER SETTINGS.

Name	R	W	T (Period)	θ	η
Divvy Bikes	20	10	1440min (1day)	20	1000
Chicago Crime	20	10	720hour (1month)	20	1000
New York Taxi	20	10	3600sec (1hour)	20	1000
Ride Austin	20	10	1440min (1day)	50	1000

C. Q2. Speed and Fitness

We compared the speed and fitness of all versions of SLICENSTITCH and the baseline methods. Fig. 4 shows how the relative fitness (i.e., fitness relative to ALS) changed over time, and Fig. 5 shows the average relative fitness and the average elapsed time for processing an event. We found Observations 2, 3, and 4.

Observation 2 (Significant Speed-ups). All versions of SLICENSTITCH updated factor matrices significantly faster than the fastest baseline. For example, $\text{SNS}_{\text{RND}}^+$ and SNS_{MAT} were up to **464 \times** and **3.71 \times faster** than CP-stream, respectively.

Observation 3 (Effect of Clipping). SNS_{VEC} and SNS_{RND} failed in some datasets due to numerical errors, as discussed in the last paragraph of Section V-C. $\text{SNS}_{\text{VEC}}^+$ and $\text{SNS}_{\text{RND}}^+$, where clipping is used, successfully addressed this problem.

Observation 4 (Comparable Fitness). All stable versions of SLICENSTITCH (i.e., $\text{SNS}_{\text{VEC}}^+$, $\text{SNS}_{\text{RND}}^+$, and SNS_{MAT}) achieved 72-100% fitness relative to the most accurate baseline.

D. Q3. Data Scalability

We measured how rapidly the total running time of different versions of SLICENSTITCH increase with respect to the number of events in Fig. 6. We found Observation 5.

Observation 5 (Linear Scalability). The total runtime of all SLICENSTITCH versions was linear in the number of events.

E. Q4. Effect of Parameters

To investigate the effect of the threshold θ for sampling on the performance of SNS_{RND} and $\text{SNS}_{\text{RND}}^+$, we measured their relative fitness and update time while varying θ from 25% to 200% of the default value in Table III.⁸ The results are reported in Fig. 7, and we found Observation 6.

Observation 6 (Effect of θ). As θ increases (i.e., more indices are sampled), the fitness of SNS_{RND} and $\text{SNS}_{\text{RND}}^+$ increases with diminishing returns, while their runtime grows linearly.

In Fig. 8, we measured the effect of the threshold η for clipping on the relative fitness of $\text{SNS}_{\text{VEC}}^+$ and $\text{SNS}_{\text{RND}}^+$, while changing η from 32 to 16,000. Note that η does not affect their speed. We found Observation 7.

⁸We set η to 500 in the Chicago Crime dataset since setting it to 1000 led to unstable results.

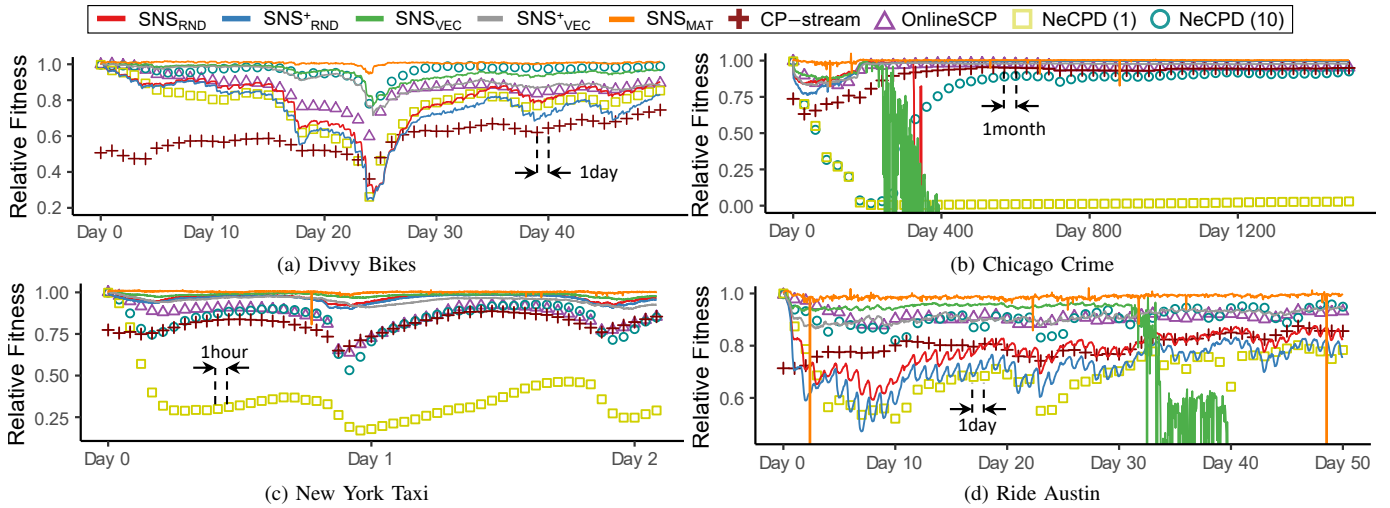


Fig. 4. Relative fitness of all versions of SLICENSTITCH and baselines over time. All versions of SLICENSTITCH (represented as lines) update outputs whenever an event occurs, while baselines (represented as dots) update outputs only once per period T .

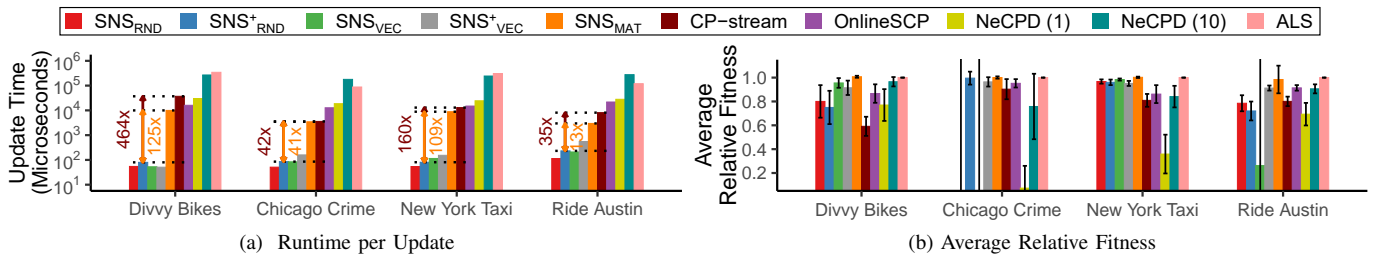


Fig. 5. All versions of SLICENSTITCH update factor matrices much faster with comparable fitness than the best baseline.

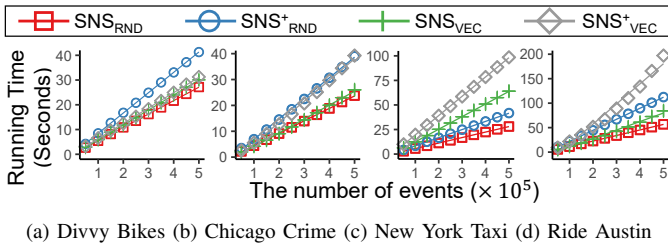


Fig. 6. The total runtime of SLICENSTITCH is linear in the number of events. While we omit SNS_{MAT} due to long execution time, it shows a similar trend.

Observation 7 (Effect of η). The fitness of SNS^+_{VEC} and SNS^+_{RND} is insensitive to η as long as η is small enough.

F. Q5. Practitioner’s Guide

Based on the above theoretical and empirical results, we provide a practitioner’s guide for SLICENSTITCH’s users.

- We do not recommend SNS_{VEC} and SNS_{RND} . They are prone to numerical errors and thus unstable.
- We recommend using the version fitting the input tensor best within your runtime budget among SNS_{MAT} , SNS^+_{VEC} , and SNS^+_{RND} . There exists a clear trade-off between their speed and fitness. In terms of speed, SNS^+_{RND} is the best followed by SNS^+_{VEC} , and SNS_{MAT} is the slowest. In terms of fitness, SNS_{MAT} is the best followed by SNS^+_{VEC} , and SNS^+_{RND} is the most inaccurate.
- If SNS^+_{RND} is chosen, we recommend increasing θ as much as possible, within your runtime budget.

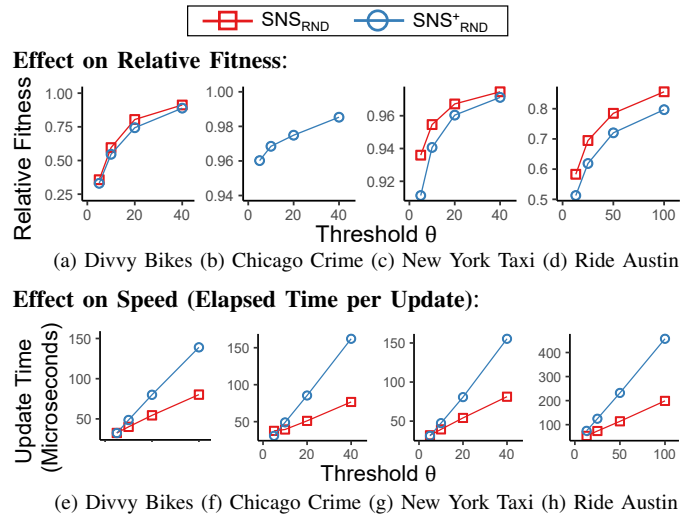
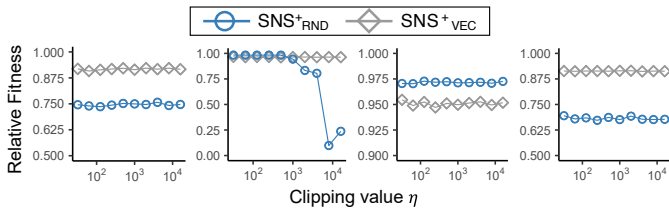


Fig. 7. Effect of θ on the performance of SNS_{RND} and SNS^+_{RND} . As θ increases, the fitness increases with diminishing returns, while the runtime grows linearly. SNS_{RND} fails in the Chicago Crime dataset due to instability.

G. Q6. Application to Anomaly Detection

We applied SNS^+_{RND} , OnlineSCP, and CP-stream to an anomaly detection task. In the New York Taxi dataset, we injected abnormally large changes (specifically, 15, which is 5 times the maximum change in 1 second in the data stream) in 20 randomly chosen entries. Then, we measured the Z scores of the errors in all entries in the latest tensor unit, where new changes arrive, as each method proceeded. After that, we investigated the top-20 Z-scores in each method. As summarized in Fig. 9, the precision, which is the same as the recall in our setting,



(a) Divvy Bikes (b) Chicago Crime (c) New York Taxi (d) Ride Austin

Fig. 8. Effects of η on the fitness of $\text{SNS}^+_{\text{VEC}}$ and $\text{SNS}^+_{\text{RND}}$. The fitness is insensitive to η , as long as it is small enough.

was highest in $\text{SNS}^+_{\text{RND}}$ and OnlineSCP. More importantly, the average time gap between the occurrence and detection of the injected anomalies was about 0.0015 seconds in $\text{SNS}^+_{\text{RND}}$, while that exceeded 1,400 seconds in the others, which have to wait until the current period ends to update CPD.

VII. RELATED WORK

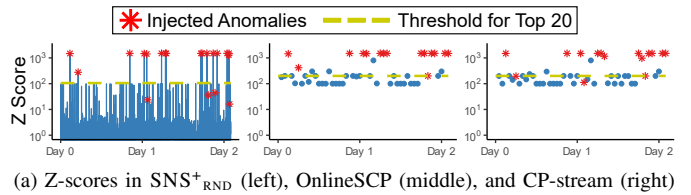
In this section, we review related work on online CP decomposition (CPD) and window-based tensor analysis. Then, we briefly discuss the relation between CPD and machine learning. See [19], [29] for more models, solvers, and applications.

A. Online Tensor Decomposition

Nion et al. [25] proposed Simultaneously Diagonalization Tracking (SDT) and Recursively Least Squares Tracking (RLST) for incremental CP decomposition (CPD) of three-mode dense tensors. Specifically, SDT incrementally tracks the SVD of the unfolded tensor, while RLST recursively updates the factor matrices to minimize the weighted squared error. A limitation of the algorithms is that they are only applicable to three-mode dense tensors. Gujral et al. [17] proposed a sampling-based method called SamBaTen for incremental CPD of three-mode dense and sparse tensors. Zhou et al. proposed onlineCP [27] and onlineSCP [16] for incremental CPD of higher-order dense tensors and sparse tensors, respectively. Smith et al. [15] proposed an online CPD algorithm that can be extended to include non-negativity and sparsity constraints. It is suitable for both sparse and dense tensors. SGD-based methods [28], [30] have also been developed for online CPD. Specifically, Ye et al. [30] proposed one for Poisson-distributed count data with missing values and Anaissi et al. [28] employed Nesterov’s Accelerated Gradient method into SGD. Sobral et al. [31] developed an online framework for subtracting background pixels from multispectral video data. However, all these algorithms process every new entry with the same time-mode index (e.g., a slice in Fig. 1a) at once. They are not applicable to continuous CPD (Problem 2), where changes in entries need to be processed instantly.

BICP [32] efficiently updates block-based CPD [33], [34] when the size of the input tensor is fixed but some existing entries change per update. It requires partitioned subtensors and their CPDs rather than the CPD of the entire input tensor.

Moreover, several algorithms have been developed for incrementally updating the outputs of matrix factorization [35], [36], Bayesian probabilistic CP factorization [37], and generalized CPD [38], when previously unknown entries are revealed afterward. They are also not applicable to continuous



(a) Z-scores in $\text{SNS}^+_{\text{RND}}$ (left), OnlineSCP (middle), and CP-stream (right)

	Precision @ Top-20	Time Gap between Occurrence and Detection
$\text{SNS}^+_{\text{RND}}$	0.80	0.0015 seconds
OnlineSCP	0.80	1601.00 seconds
CP-stream	0.70	1424.57 seconds

(b) Numerical Comparison with Baselines

Fig. 9. SLICENSTITCH (spec., $\text{SNS}^+_{\text{RND}}$) detects injected anomalies in the New York Taxi dataset much faster with comparable accuracy than baselines.

CPD (Problem 2), where even increments and decrements of revealed entries need to be handled (see Definition 6).

Lastly, it is worth mentioning that there have been several studies on approximation properties of some offline CPD algorithms. Haupt et al. [39] proved a sufficient condition for a sparse random projection technique to solve the low-rank tensor regression problem efficiently with an approximation quality. Song et al. [40] showed that an importance-sampling based orthogonal tensor decomposition algorithm achieves a sublinear time complexity with provable guarantees. To the best of our knowledge, however, there has been limited work on theoretical properties of online CPD of tensor streams.

B. Window-based Tensor Analysis

Sun et al. [22], [23] first suggested the concept of window-based tensor analysis (WTA). Instead of analyzing the entire tensor at once, they proposed to analyze a temporally adjacent subtensor within a time window at a time, while sliding the window. Based on the sliding window model, they devised an incremental Tucker decomposition algorithm for tensors growing over time. Xu et al. [24] also suggested a Tucker decomposition algorithm for sliding window tensors and used it to detect anomalies in road networks. Zhang et al. [26] used the sliding window model with exponential weighting for robust Bayesian probabilistic CP factorization and completion. Note that all these studies assume a time window moves ‘discretely’, while in our continuous tensor model, a time window moves ‘continuously’, as explained in Section IV.

C. Relation to Machine Learning

CP decomposition (CPD) has been a core building block of numerous machine learning (ML) algorithms, which are designed for classification [41], weather forecast [14], recommendation [11], stock price prediction [13], to name a few. Moreover, CPD has proven useful for outlier removal [42], [43], imputation [12], [43], and dimensionality reduction [19], and thus it can be used as a preprocessing step of ML algorithms, many of which are known to be vulnerable to outliers, missings, and the curse of dimensionality. We refer the reader to [44] for more roles of tensor decomposition for ML. By making the core building block “real-time”, our work represents a step towards real-time ML. Moreover, SLICENSTITCH can directly be used as a preprocessing step of existing streaming ML algorithms.

VIII. CONCLUSION

In this work, we propose SLICENSTITCH, aiming to make tensor analysis “real-time” and applicable to time-critical applications. We summarize our contributions as follows:

- **New data model:** We propose the continuous tensor model and its efficient event-driven implementation (Section IV). With our CPD algorithms, it achieves near real-time updates, high fitness, and a small number of parameters (Fig. 1).
- **Fast online algorithms:** We propose a family of online algorithms for CPD in the continuous tensor model (Section V). They update factor matrices in response to changes in an entry up to $464\times$ faster than online competitors, with fitness even comparable (spec., 72-100%) to offline competitors (Fig. 5). We analyze their complexities (Theorems 3-7).
- **Extensive experiments:** We evaluate the speed, fitness, and scalability of our algorithms on 4 real-world sparse tensors. We analyze the effects of hyperparameters. The results indicate a clear trade-off between speed and fitness, based on which we provide practitioner’s guides (Section VI).

Reproducibility: The code and datasets used in the paper are available at <https://github.com/DMLab-Tensor/SliceNStitch>.

ACKNOWLEDGEMENT

This work was supported by Samsung Electronics Co., Ltd., Disaster-Safety Platform Technology Development Program of the National Research Foundation of Korea (NRF) funded by the Ministry of Science and ICT (No. 2019M3D7A1094364), and Institute of Information & Communications Technology Planning & Evaluation (IITP) grant funded by the Korea government (MSIT) (No. 2019-0-00075, Artificial Intelligence Graduate School Program (KAIST)).

REFERENCES

- [1] L. Zhao and M. J. Zaki, “Tricuster: an effective algorithm for mining coherent clusters in 3d microarray data,” in *SIGMOD*, 2005.
- [2] D. Koutra, E. E. Papalexakis, and C. Faloutsos, “Tensorsplat: Spotting latent anomalies in time,” in *PCI*, 2012.
- [3] Y. Cai, H. Tong, W. Fan, P. Ji, and Q. He, “Facets: Fast comprehensive mining of coevolving high-order time series,” in *KDD*, 2015.
- [4] B. W. Bader, M. W. Berry, and M. Browne, “Discussion tracking in enron email using parafac,” in *Survey of Text Mining II*. Springer, 2008, pp. 147–163.
- [5] D. Bruns-Smith, M. M. Baskaran, J. Ezick, T. Henretty, and R. Lethin, “Cyber security through multidimensional data decompositions,” in *CYBERSEC*, 2016.
- [6] H. Fanaee-T and J. Gama, “Tensor-based anomaly detection: An interdisciplinary survey,” *Knowledge-Based Systems*, vol. 98, pp. 130–147, 2016.
- [7] F. L. Hitchcock, “The expression of a tensor or a polyadic as a sum of products,” *Journal of Mathematics and Physics*, vol. 6, no. 1-4, pp. 164–189, 1927.
- [8] J. D. Carroll and J.-J. Chang, “Analysis of individual differences in multidimensional scaling via an n-way generalization of “eckart-young” decomposition,” *Psychometrika*, vol. 35, no. 3, pp. 283–319, 1970.
- [9] R. A. Harshman, “Parafac2: Mathematical and technical notes,” *UCLA working papers in phonetics*, vol. 22, no. 3044, p. 122215, 1972.
- [10] L. R. Tucker, “Some mathematical notes on three-mode factor analysis,” *Psychometrika*, vol. 31, no. 3, pp. 279–311, 1966.
- [11] L. Yao, Q. Z. Sheng, Y. Qin, X. Wang, A. Shemshadi, and Q. He, “Context-aware point-of-interest recommendation using tensor factorization with social regularization,” in *SIGIR*, 2015.
- [12] K. Shin, L. Sael, and U. Kang, “Fully scalable methods for distributed tensor factorization,” *TKDE*, vol. 29, no. 1, pp. 100–113, 2016.
- [13] A. Spelta, “Financial market predictability with tensor decomposition and links forecast,” *Applied network science*, vol. 2, no. 1, p. 7, 2017.
- [14] J. Xu, X. Liu, T. Wilson, P.-N. Tan, P. Hatami, and L. Luo, “Muscat: Multi-scale spatio-temporal learning with application to climate modeling,” in *IJCAI*, 2018.
- [15] S. Smith, K. Huang, N. D. Sidiropoulos, and G. Karypis, “Streaming tensor factorization for infinite data sources,” in *SDM*, 2018.
- [16] S. Zhou, S. Erfani, and J. Bailey, “Online cp decomposition for sparse tensors,” in *ICDM*, 2018.
- [17] E. Gujral, R. Pasricha, and E. E. Papalexakis, “Sambaten: Sampling-based batch incremental tensor decomposition,” in *SDM*, 2018.
- [18] R. Pasricha, E. Gujral, and E. E. Papalexakis, “Adaptive granularity in tensors: A quest for interpretable structure,” *arXiv preprint arXiv:1912.09009*, 2019.
- [19] T. G. Kolda and B. W. Bader, “Tensor decompositions and applications,” *SIAM review*, vol. 51, no. 3, pp. 455–500, 2009.
- [20] (2020) Supplementary document. [Online]. Available: <https://github.com/DMLab-Tensor/SliceNStitch/blob/master/doc/supplementary.pdf>
- [21] R. A. Harshman *et al.*, “Foundations of the parafac procedure: Models and conditions for an” explanatory” multimodal factor analysis,” 1970.
- [22] J. Sun, S. Papadimitriou, and S. Y. Philip, “Window-based tensor analysis on high-dimensional and multi-aspect streams,” in *ICDM*, 2006.
- [23] J. Sun, D. Tao, S. Papadimitriou, P. S. Yu, and C. Faloutsos, “Incremental tensor analysis: Theory and applications,” *ACM Transactions on Knowledge Discovery from Data*, vol. 2, no. 3, pp. 1–37, 2008.
- [24] M. Xu, J. Wu, H. Wang, and M. Cao, “Anomaly detection in road networks using sliding-window tensor factorization,” *T-ITS*, vol. 20, no. 12, pp. 4704–4713, 2019.
- [25] D. Nion and N. D. Sidiropoulos, “Adaptive algorithms to track the parafac decomposition of a third-order tensor,” *TSP*, vol. 57, no. 6, pp. 2299–2310, 2009.
- [26] Z. Zhang and C. Hawkins, “Variational bayesian inference for robust streaming tensor factorization and completion,” in *ICDM*, 2018.
- [27] S. Zhou, N. X. Vinh, J. Bailey, Y. Jia, and I. Davidson, “Accelerating online cp decompositions for higher order tensors,” in *KDD*, 2016.
- [28] A. Ainaissi, B. Suleiman, and S. M. Zandavi, “Necpd: An online tensor decomposition with optimal stochastic gradient descent,” *arXiv preprint arXiv:2003.08844*, 2020.
- [29] E. E. Papalexakis, C. Faloutsos, and N. D. Sidiropoulos, “Tensors for data mining and data fusion: Models, applications, and scalable algorithms,” *ACM Transactions on Intelligent Systems and Technology*, vol. 8, no. 2, pp. 1–44, 2016.
- [30] C. Ye and G. Mateos, “Online tensor decomposition and imputation for count data,” in *DSW*, 2019.
- [31] A. Sobral, S. Javed, S. Ki Jung, T. Bouwmans, and E.-h. Zahzah, “Online stochastic tensor decomposition for background subtraction in multispectral video sequences,” in *ICCVW*, 2015.
- [32] S. Huang, K. S. Candan, and M. L. Sapino, “Bicp: block-incremental cp decomposition with update sensitive refinement,” in *CIKM*, 2016.
- [33] A. H. Phan and A. Cichocki, “Parafac algorithms for large-scale problems,” *Neurocomputing*, vol. 74, no. 11, pp. 1970–1984, 2011.
- [34] X. Li, S. Huang, K. S. Candan, and M. L. Sapino, “2pcp: Two-phase cp decomposition for billion-scale dense tensors,” in *ICDE*, 2016.
- [35] X. He, H. Zhang, M.-Y. Kan, and T.-S. Chua, “Fast matrix factorization for online recommendation with implicit feedback,” in *SIGIR*, 2016.
- [36] R. Devooght, N. Kourtellis, and A. Mantrach, “Dynamic matrix factorization with priors on unknown values,” in *KDD*, 2015.
- [37] Y. Du, Y. Zheng, K.-c. Lee, and S. Zhe, “Probabilistic streaming tensor decomposition,” in *ICDM*, 2018.
- [38] S. Zhou, S. M. Erfani, and J. Bailey, “Sced: A general framework for sparse tensor decomposition with constraints and elementwise dynamic learning,” in *ICDM*, 2017.
- [39] J. Haupt, X. Li, and D. P. Woodruff, “Near optimal sketching of low-rank tensor regression,” in *NIPS*, 2017.
- [40] Z. Song, D. P. Woodruff, and H. Zhang, “Sublinear time orthogonal tensor decomposition,” in *NIPS*, 2016.
- [41] S. Rendle, “Factorization machines,” in *ICDM*, 2010.
- [42] M. Najafi, L. He, and S. Y. Philip, “Outlier-robust multi-aspect streaming tensor completion and factorization,” in *IJCAI*, 2019.
- [43] D. Lee and K. Shin, “Robust factorization of real-world tensor streams with patterns, missing values, and outliers,” in *ICDE*, 2021.
- [44] N. D. Sidiropoulos, L. De Lathauwer, X. Fu, K. Huang, E. E. Papalexakis, and C. Faloutsos, “Tensor decomposition for signal processing and machine learning,” *TSP*, vol. 65, no. 13, pp. 3551–3582, 2017.